Appendix PA

Attachment TFIELD

Table of Contents

List of Figures

List of Tables

TFIELD-1.0 OVERVIEW OF T-FIELD DEVELOPMENT, CALIBRATION, AND MODIFICATION PROCESS

Modeling the transport of radionuclides through the Culebra Dolomite Member of the Rustler Formation is one component of the Performance Assessment (PA) performed for the Waste Isolation Pilot Plant (WIPP) Compliance Recertification Application (CRA). This transport modeling requires a model of groundwater flow through the Culebra. This Attachment describes the process used to develop and calibrate the transmissivity (T) fields for the Culebra, and then modify them for the possible effects of potash mining for use in flow modeling for the CRA-2004.

The work described in this attachment was performed under two Sandia National Laboratories Analysis Plans (APs): AP-088 (Beauheim 2002a) and AP-100 (Leigh et al. 2003). AP-088 (Analysis Plan for the Evaluation of the Effects of Head Changes on Calibration of Culebra Transmissivity Fields) dealt with the development, calibration, and modification for potash mining of the T fields. AP-100 (Analysis Plan for Calculations of Culebra Flow and Transport: Compliance Recertification Application) included the development of T-field acceptance criteria, as well as radionuclide-transport calculations not described herein.

The starting point in the T-field development process was to assemble information on geologic factors that might affect Culebra T (Section 2.0 of this attachment). These factors include dissolution of the upper Salado Formation, the thickness of overburden above the Culebra, and the spatial distribution of halite in the Rustler Formation above and below the Culebra. Geologic information is available from hundreds of oil and gas wells and potash exploration holes in the vicinity of the WIPP site, while T values are available from only 46 well locations. Details of the geologic data compilation are given in Powers (2002a, 2002b, 2003), and summarized below in Section 2.0 of this attachment.

A two-part “geologically based” approach was then used to generate Culebra base T fields. In the first part (Section 3.0 of this attachment), a conceptual model for geologic controls on Culebra T was formalized, and the hypothesized geologic controls were regressed against Culebra T data to determine linear regression coefficients. The regression includes one continuously varying function, Culebra overburden thickness, and three indicator functions that assume values of 0 or 1 depending on the occurrence of open, interconnected fractures, Salado dissolution, and the presence or absence of halite in units bounding the Culebra.

In the second part (Section 4.0 of this attachment), a method was developed for applying the linear regression model to predict Culebra T across the WIPP area. The regression model was combined with the maps of geologic factors to create 500 stochastically varying Culebra base T fields. Details about the development of the regression model and the creation of the base T fields are given in Holt and Yarbrough (2002, 2003a, 2003b).

By the nature of regression models, the base T fields do not honor the measured T values at the measurement locations. Therefore, before these base T fields could be used in a flow model, they had to be conditioned to the measured T values. This conditioning is described in McKenna and Hart (2003a, 2003b) and summarized in Section 5.0 of this attachment. Section 6.0 of this attachment presents details on the modeling approach used to calibrate the T fields to both steady-state heads and transient drawdown measurements. Heads measured in late 2000 were used to represent steady-state conditions in the Culebra, and drawdown responses in 40 wells to pumping in 7 wells were used to provide transient calibration data. Details on the heads and drawdown data used are described in Beauheim (2002b; 2003a). Assumptions made in modeling, the definition of an initial head distribution, assignment of boundary conditions, discretization of the spatial and temporal domain, weighting of the observations, and the use of PEST in combination with MODFLOW-2000 to calibrate the T fields using a pilot-point method are described in McKenna and Hart (2003a, 2003b) and summarized in Section 6.0 of this attachment.

Section 7.0 of this attachment addresses the development and application of acceptance criteria for the T fields. Acceptance was based on a combination of objective fit to the calibration data and providing travel time results consistent with the cumulative distribution function (CDF) of travel times from the 23 best-calibrated T fields (Beauheim 2003b). Of the 146 T fields that went through the calibration process, 121 T fields were judged adequate for further use, with the 100 best T fields selected for use in the CRA-2004 transport calculations.

Section 8.0 of this attachment provides summary statistics and other information for the 121 T fields that were judged to be acceptably calibrated. Particle tracks from a point above the center of the WIPP disposal panels to the land withdrawal boundary are shown, along with information on the model fits to steady-state heads, identification of the most sensitive pilot point locations, and characteristics of an ensemble average T field. This information is summarized from McKenna and Hart (2003b).

Section 9.0 of this attachment discusses the modification of the T fields to account for the effects of potash mining both within and outside the WIPP land withdrawal boundary. Mining-affected areas were delineated, random transmissivity multipliers were applied to Ts in those areas, and particle tracks and travel times were determined (Lowry 2003). The flow fields produced by these mining-affected T fields are input to SECOTP2D for the CRA-2004 radionuclide-transport calculations.

Section 10.0 of this attachment provides a brief summary of this attachment.

TFIELD-2.0 DEVELOPMENT OF MAPS OF GEOLOGIC FACTORS

Beauheim and Holt (1990), among others, suggested three geologic factors that might be related to the transmissivity of the Culebra in the vicinity of the WIPP site:

1. thickness (or erosion) of overburden above the Culebra,
2. dissolution of the upper Salado , and
3. spatial distribution of halite in the Rustler Formation below and above the Culebra.

Culebra transmissivity is inversely related to thickness of overburden because stress relief associated with erosion of overburden leads to fracturing and opening of preexisting fractures. Culebra transmissivity is high where dissolution of the upper Salado has occurred and the

Culebra has subsided and fractured. Culebra transmissivity is observed to be low where halite is present in overlying and/or underlying mudstones. Presumably, high Culebra T leads to dissolution of nearby halite (if any). Hence, the presence of halite in mudstones above and/or below the Culebra can be taken as an indicator for low Culebra transmissivity.

Maps were developed for each of these factors using drillhole data of different types. The general area for the geologic study comprised 12 townships, located in townships T21S to T24S, ranges R30-32E (the WIPP site lies in T22S, R31E). The original sources of geologic data for this analysis are mainly Powers and Holt (1995) and Holt and Powers (1988) and new information derived by log interpretation by Powers (2002a, 2003b, 2003). All of the data are either included or summarized in the references cited above, and can be independently checked; basic data reports are available for WIPP drillholes, geophysical logs for oil and gas wells are available commercially or at offices of the Oil Conservation Division (New Mexico) in Artesia and Hobbs, and potash drillhole information is in files that can be accessed for stratigraphic information at the Bureau of Land Management (BLM), Carlsbad, NM. No proprietary data are included.

Factor A is represented by a structure contour map of the elevation of the top of the Culebra (Figure TFIELD-1) that can be digitized and then subtracted from a digital elevation model (DEM) of the land surface to obtain the thickness of overburden. Factor B is represented on a map as an approximate margin of the area beginning to be affected by dissolution of the upper Salado (Figure TFIELD-2). Factor C is delineated on a map by lines that represent as nearly as possible the boundaries of the occurrence of halite in the Los Medaños, Tamarisk, and Forty-niner Members of the Rustler Formation in the study domain (Figure TFIELD-3).

With respect to Factor B, the upper Salado has been dissolved, and presumably is still dissolving, along the eastern margin of Nash Draw. On the basis of limited core information, Holt and Powers (1988) suggested that formations overlying the dissolving upper Salado in Nash Draw are affected in proportion to the amount of Salado dissolution. The most direct way to estimate the spatial distribution of dissolution is to have cores of the upper Salado and basal Rustler and knowledge of the thickness to marker beds (MBs) in the upper Salado. The upper Salado has not been cored frequently, but geophysical logs from oil and gas wells, and descriptive logs of cores or cuttings from potash drillholes, provide a considerable amount of evidence of the thickness of the lower Rustler and upper Salado, even though cores and cuttings are no longer available from potash industry drillholes.

Potash industry geological logs examined at the BLM in Carlsbad, NM~~,~~ are quite variable in the quality of description and the stratigraphic interval described. Drillhole logs from the 1930s and 1950s typically are the most descriptive; recent drillhole logs are commonly useless for this project because no strata are described above portions of the McNutt potash zone of the Salado, near the middle of the formation.

The top of the Culebra and the base of the Vaca Triste Sandstone Member in the upper Salado are the most consistent stratigraphic markers spanning the upper Salado that are recognizable across various types of records. As a guide to the limits or bounds of upper Salado dissolution, a map of the thickness from top of Culebra to base of Vaca Triste was prepared (Powers 2003). In conjunction with previous work by Powers and Holt (1995) and the evidence of the structure of the top of Culebra (see Figure TFIELD-1), an approximate boundary of dissolution was drawn as shown in Figure TFIELD-2.

With respect to Factor C, the boundaries of where halite is found in the three non-carbonate members of the Rustler have been drawn several times on the basis of different borehole data sets and different data types (e.g., core data and geophysical logs). For the most part, the different versions of the boundaries do not vary significantly. In the map shown in Figure TFIELD-3, the margins are based principally on the work of Powers and Holt (1995), which is a continuation of work reported by Holt and Powers (1988). As discussed in Powers and Holt (1995), the boundaries drawn here vary slightly from those drawn by Snyder (1985) based on core data for two reasons: (1) the Los Medaños Member (Powers and Holt 1999; formerly called the unnamed lower member) is here divided into two separate halite-bearing units (Powers and Holt 2000), and (2) geophysical log signatures are now used to identify halite in areas where cores are not available. Figure TFIELD-3 includes a stratigraphic sketch showing the relationship of halite-bearing strata to other strata in the Rustler. Following the convention established by Holt and Powers (1988), the mudstone/halite (M/H) strata are numbered consecutively starting at the base of the Rustler.

The margins for halite have now been drawn in the area north of the WIPP site around the northeastern arm of Nash Draw based on the descriptions of halite encounters in the Rustler Formation in potash drillholes. In addition, a few areas have been modified (from Powers and Holt 1995) to the south and west of the WIPP based on the records from potash drillholes as well as the records of drilling H-12 and H-17 for the WIPP.

In 12 potash drillholes, halite was reported above the upper contacts of the Culebra or Magenta Dolomite Members. The boundaries for M3/H3 and M4/H4 margins (i.e., the spatial limits of where halite is found in the mudstone intervals) have been drawn north of the WIPP based on these data. The depth below the Culebra at which halite was reported has also been used to draw the boundaries of the lower (M1/H1) or the upper (M2/H2) halite-bearing units of the Los Medaños in this area. Anhydrite A1 divides the M1/H1 (below) and M2/H2 (above) intervals. M2 (no halite) is about 3 m (10 ft) thick. If halite is reported within about 3 m (10 ft) of the base of Culebra or is clearly above A1, H2 is considered to be present. The M1/H1 interval is about 33-37 m (110-120 ft) thick at the WIPP site. In potash drillholes north of the WIPP site, where halite was reported less than 33 m (110 ft) below the Culebra, H1 is present. Within the zone for H1, other drillholes frequently reveal halite less than 33 m (110 ft) below the Culebra.

It should be noted that the report of "top of salt" or first salt in records for potash drillholes does not consistently mean the same thing and is frequently not the uppermost halite. It may instead mean the first halite that is encountered after coring begins or the first unit that is dominantly halite. Detailed inspection of logs sometimes shows halite described from cuttings, with a summary report of "top of salt" much deeper. In some cases, it appears "top of salt" is an estimate of where the Salado-Rustler contact should be.

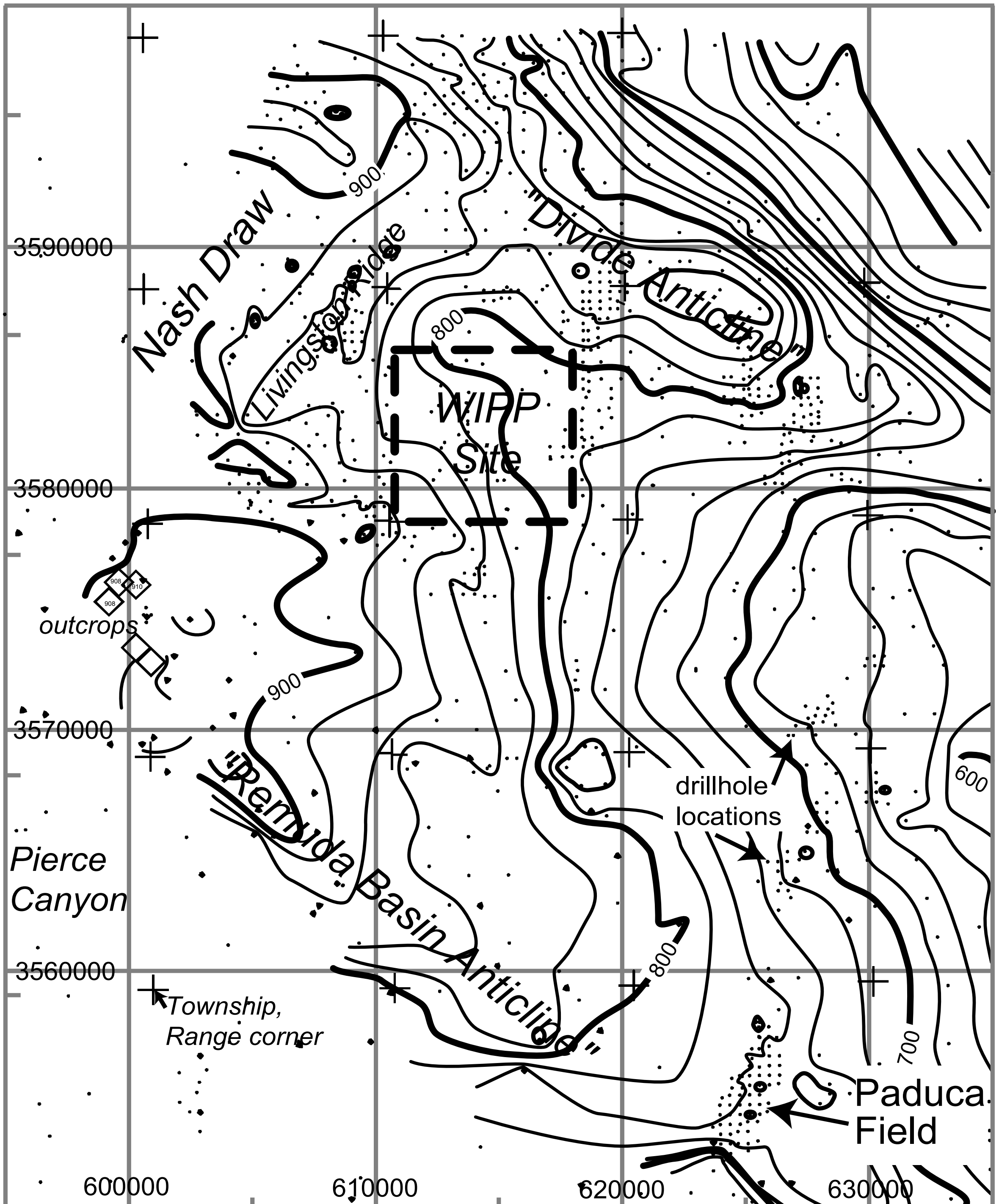

Explanation
UTM coordinates (m) for Zone 13 (NAD27) are provided for easting and northing.
The contours for the elevation of the top of the Culebra are in meters (m) above mean sea level (amsl) (after Powers et al. 2003). Contour interval is 20 m.

Figure TFIELD-1. Structure Contour Map for the Top of the Culebra

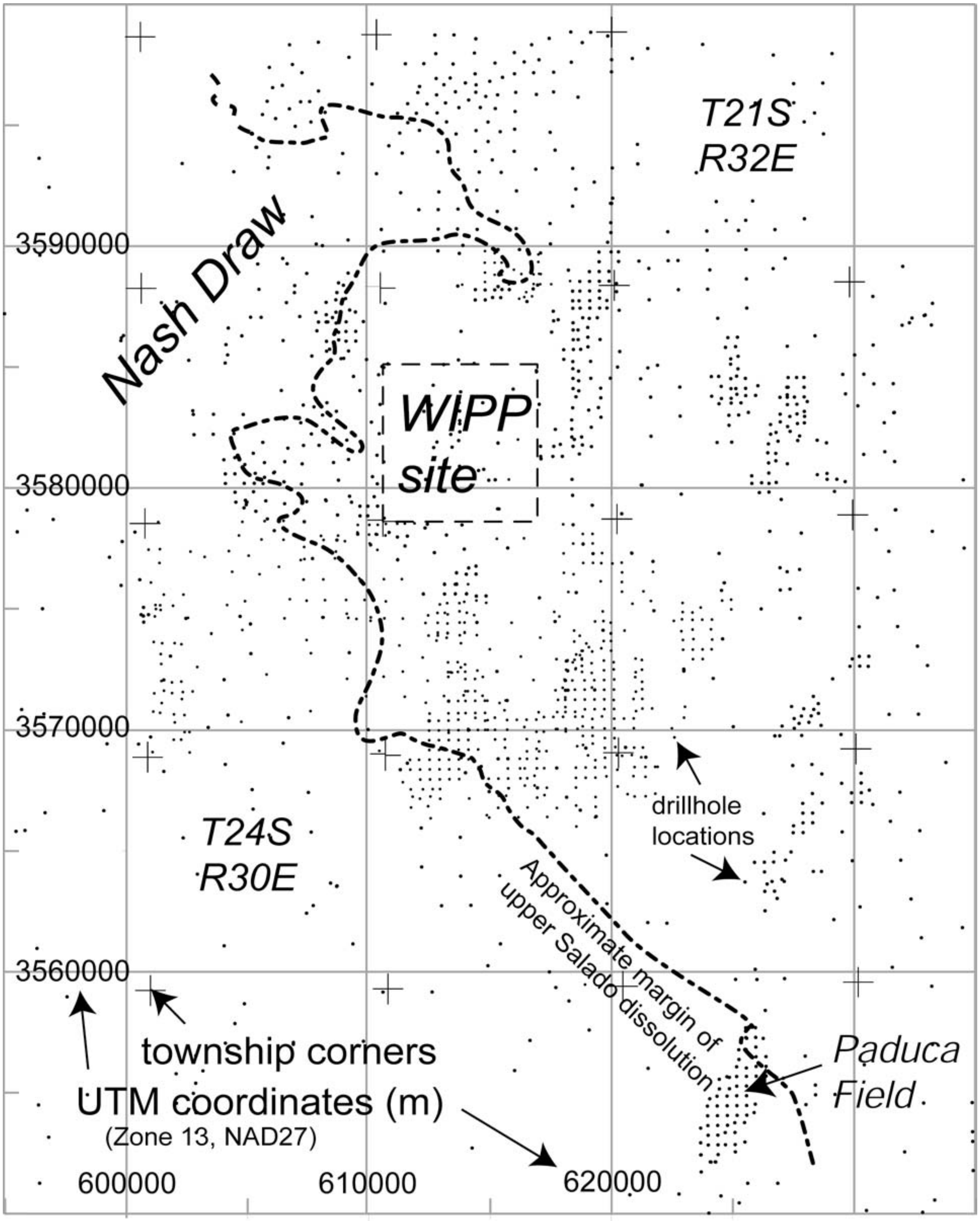

Figure TFIELD-2. Salado Dissolution Margin

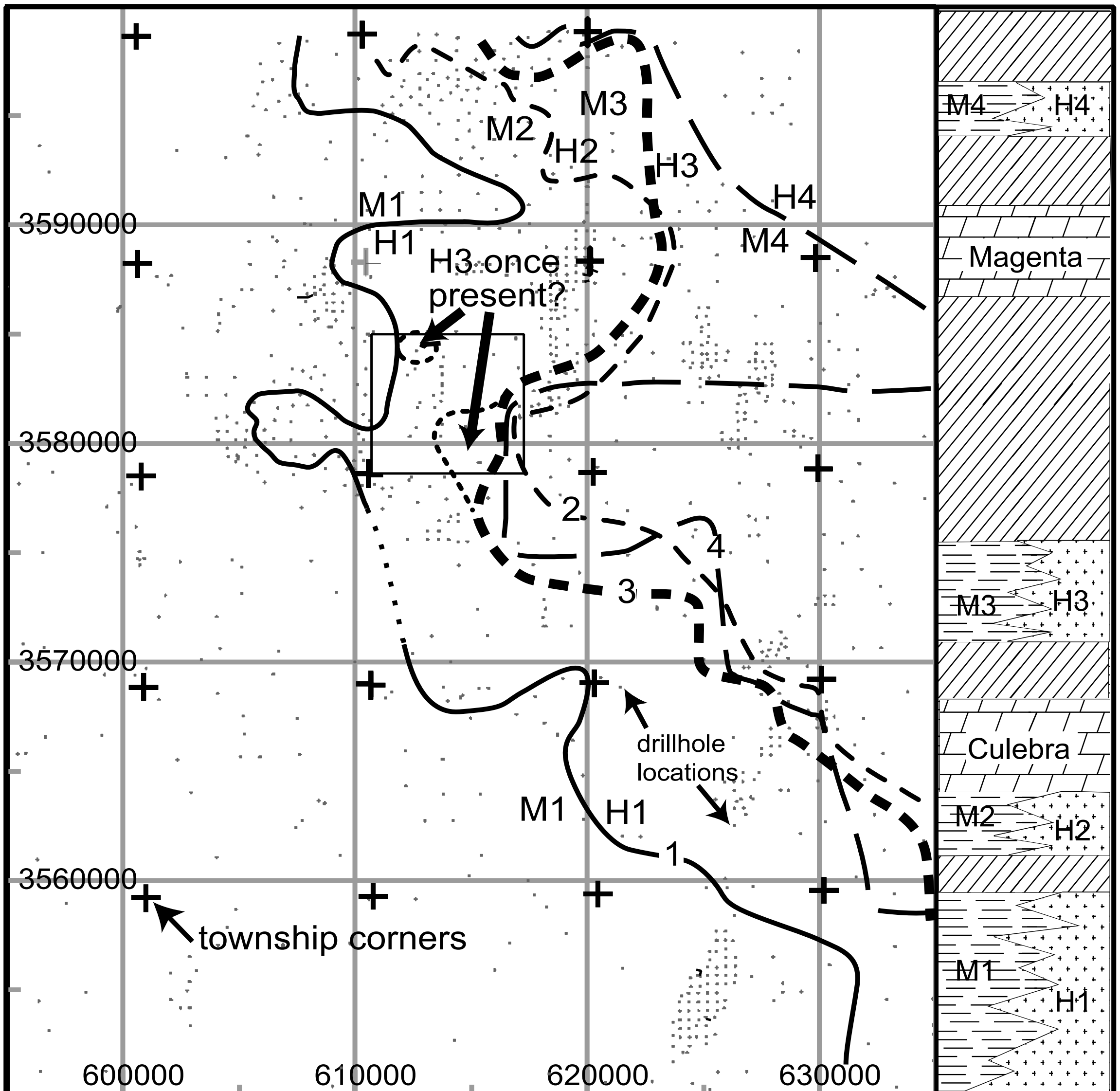

Explanation

M#, H# indicate mudstone and halitic facies on each side of estimated halite margin (numbered line on map) for stratigraphic intervals as indicated in the column to the right (key on Figure TFIELD-4).

UTM coordinates (m) for Zone 13 (NAD27) are provided for easting and northing.

Two zones within the WIPP site boundary ("H3 once present?") indicate where halite may have been present west of the current boundary of H3 (marked by ▬ ▬ ▬ ▬ ▪).

Figure TFIELD-3. Rustler Halite Margins. See Figure TFIELD-4 for key to stratigraphic column.

Halite margins in the Rustler Formation are interpreted as mainly due to depositional limits of saltpan environments and syndepositional removal of some halite exposed in saline mud flat deposits (Holt and Powers 1988). The halite margins are expected to be the locus of halite dissolution, if any, since the Rustler was deposited. Facies including halite beds or halite cements are expected to be less permeable than the equivalent mudstone facies. As a consequence, the margin is more likely to be attacked by advection and diffusion at the margin, from the mudstone facies side of the margin. In addition, removing halite along the margin as the saltpan margin fluctuates is likely to introduce some vertical and horizontal discontinuities that persist after lithification and are not created where the saltpan persisted. Water in adjacent units or in the mudstone unit likely has more pathways along these margins, increasing the likelihood that the margins will be the locus of dissolution. Recent findings of a narrow margin along which halite is dissolved from the upper Salado (Powers et al. 2003) are consistent with the expectation that halite margins in the Rustler would be the locus of dissolution.

Two areas have been identified where halite appears to have been dissolved from the M3/H3 interval after deposition of the Rustler. These areas are shown with the annotation "H3 once present?" on Figure TFIELD-3. In the vicinity of drillhole H-19b0 and south (the southern area shown), cores of several WIPP drillholes show brecciation of the upper Tamarisk Member anhydrite in response to dissolution. Another area of dissolution, previously discussed in Holt and Powers (1988), Powers and Holt (1995), and Beauheim and Holt (1990), is around WIPP-13 (the northern area shown), and may represent an outlier of salt left behind during syndepositional removal of halite from the M3 areas west of the WIPP site (Powers and Holt 2000). These areas have not been extended interpretively on Figure TFIELD-3 as was done in Beauheim and Holt (1990), but are limited to the vicinities of the locations at which evidence of dissolution has been directly observed.

Because of the position of M2/H2 directly beneath the Culebra, dissolution of H2 might be expected to have a strong influence on Culebra T. However, the H2 depositional margin is largely east of the WIPP site, barely crossing the southern portion of the eastern WIPP site boundary (Figure TFIELD-3). H2 dissolution does not appear to be a factor affecting Culebra T in any hydrology test well for WIPP, but there are no direct observations along the H2 margin.

TFIELD-3.0 DEVELOPMENT OF MODEL RELATING CULEBRA T TO GEOLOGIC FACTORS

Holt and Powers (1988), Powers and Holt (1990), Beauheim and Holt (1990), and Holt (1997) have described the geology and geologic history of the Culebra. The following model is developed from their work and is consistent with their interpretations. It is important to note that this work follows Holt (1997) and assumes that variability in Culebra T is due strictly to post-depositional processes. Throughout the following discussion, the informal stratigraphic subdivisions of Holt and Powers (1988) are used to identify geologic units within the Rustler Formation (Figure TFIELD-4).

The spatial distribution of Culebra T on a regional scale is a function of a series of deterministic geologic controls, including Culebra overburden thickness, dissolution of the upper Salado Formation, and the occurrence of halite in units above or below the Culebra. Each of these

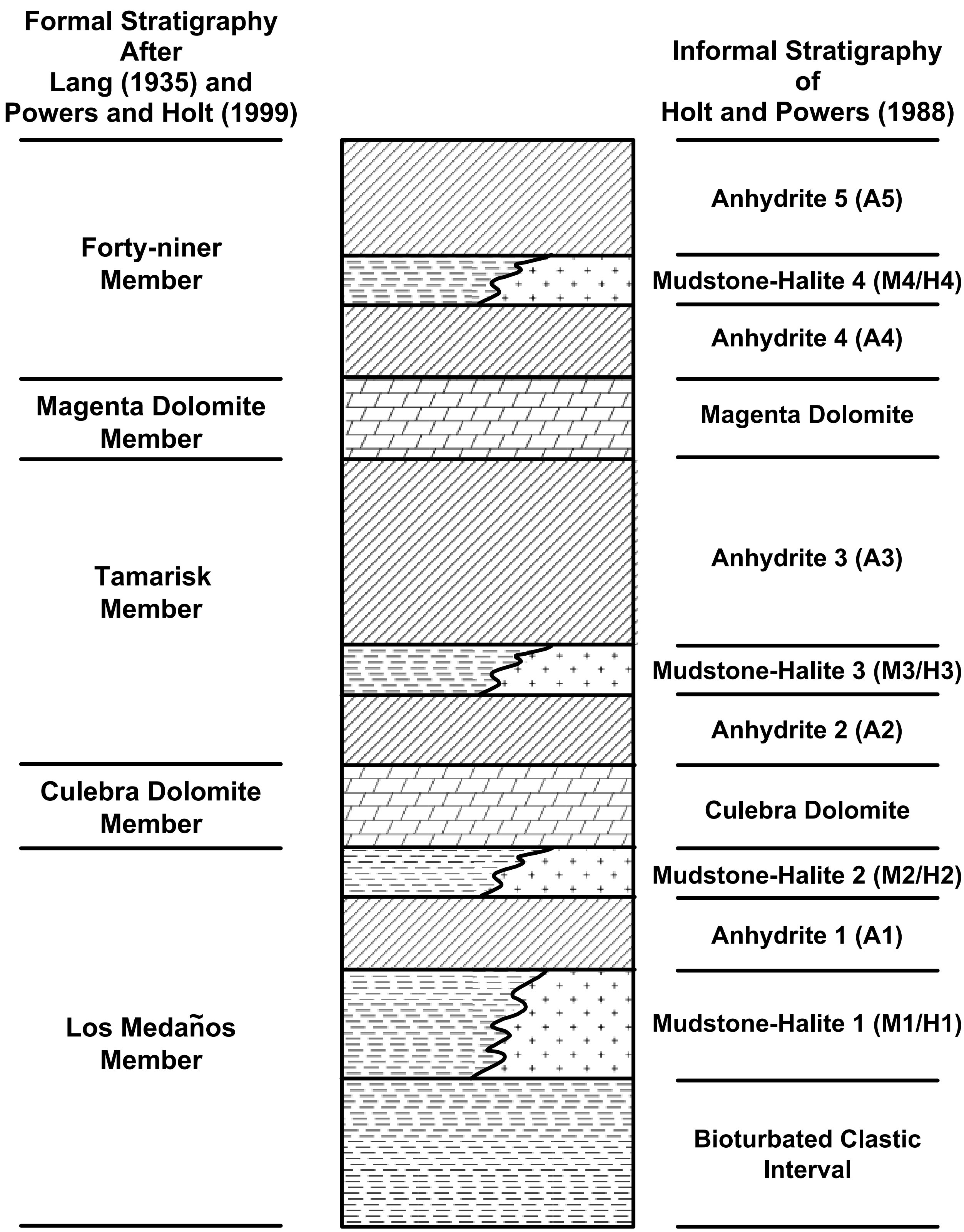

Figure TFIELD-4. Stratigraphic Subdivisions of the Rustler Formation

geologic controls can be determined at any location using geological map data. In the region between the margin of upper Salado dissolution and the margin of halite occurrence above the Culebra, which includes the WIPP site, however, high-T regions occur that cannot be predicted using geologic data. These high-T zones are treated stochastically, using what is termed a fracture-interconnectivity indicator.

In the following paragraphs, the fracture-interconnectivity indicator is defined, and then the specifics of each hypothesized control on Culebra T are outlined. Finally, a linear model relating these controls to Culebra T is presented that provides an excellent fit to the available data, is testable, and is consistent with our understanding of Culebra geology.

TFIELD-3.1 Fracture Interconnection

Culebra T data show a bimodal distribution (Figure TFIELD-5). Interpretations of hydraulic tests (e.g., Beauheim and Ruskauff 1998) and observations of the presence or absence of open fractures in core show the bimodal T distribution to be the result of hydraulically significant fractures. Some degree of fracturing is evident in all Culebra cores, but the fractures tend to be filled with gypsum at locations where the T inferred from hydraulic tests is less than approximately 4×10^{-6} m^2/s ($\log_{10}$ = -5.4). Where $\log_{10}$ T (m^2/s) is greater than –5.4, hydraulic tests show double-porosity responses and open fractures are observed in core. Therefore, a fracture-interconnectivity indicator is defined based on a cutoff of $\log_{10}$ T (m^2/s) = -5.4:

$$I_f = \begin{cases} 1 & \log_{10} T(m^2/s) > -5.4 \\ 0 & \log_{10} T(m^2/s) \le -5.4 \end{cases} \quad (1)$$

Open, interconnected fractures and high Ts occur in regions affected by Salado dissolution (e.g., Nash Draw) and in areas west of the M3/H3 margin where gypsum fracture fillings are absent.

TFIELD-3.2 Overburden Thickness

An inverse relationship exists between Culebra overburden thickness and T. At the WIPP wells for which T data are available, the Culebra overburden thickness ranges from 3.7 m (at WIPP-29) to 414.5 m (at H-10) (Mercer 1983), increasing from west to east. Overburden thickness is a metric for two different controls on Culebra T. First, fracture apertures are limited by overburden thickness (e.g., Currie and Nwachukwu 1974), which should lead to lower T where Culebra depths are great (Beauheim and Holt 1990; Holt 1997). Second, erosion of overburden leads to changes in stress fractures, and the amount of Culebra fracturing increases as the overburden thickness decreases (Holt 1997). Holt (1997) estimates that at least 350 m of overburden has been eroded at the center of the WIPP site (where the Culebra is at a depth of approximately 214 m) since the end of the Triassic, with more erosion occurring west of the site center where overburden (chiefly the Dewey Lake) is thinner and less erosion occurring to the east where Triassic deposits are thicker.

TFIELD-3.3 Salado Dissolution

In regions north, south, and west of the WIPP site, Cenozoic dissolution has affected the upper Salado Formation (Figure TFIELD-2). Where this dissolution has occurred, the rocks overlying the Salado, including the Culebra, are strained (leading to larger apertures in existing fractures),

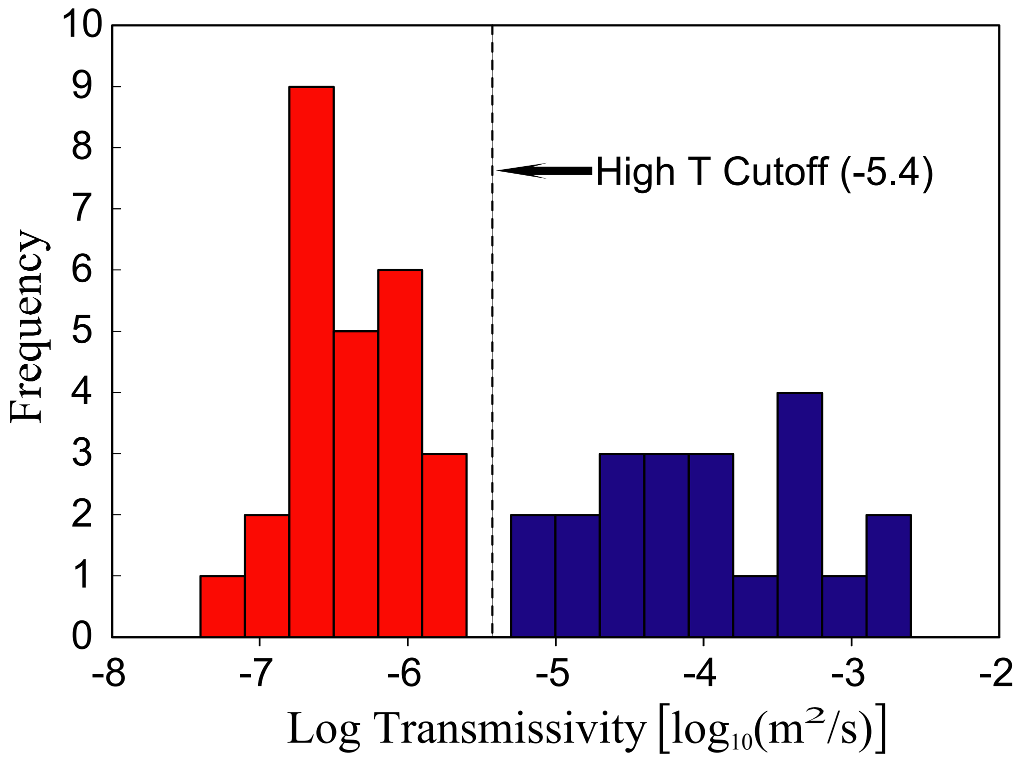

Figure TFIELD-5. Histogram of Log_{10} Culebra T. Data from DOE (1996), Beauheim and Ruskauff (1998), and Beauheim (2002c)

fractured, collapsed, and brecciated (e.g., Beauheim and Holt 1990; Holt 1997). All WIPP wells within the upper-Salado-dissolution zone fall within the high-T population, and all regions affected by Salado dissolution are expected to have well-interconnected fractures and high T.

TFIELD-3.4 Halite Overlying the Culebra

All wells (e.g., H-12 and H-17) located where halite occurs in the M3/H3 interval of the Tamarisk (Figure TFIELD-3) show low T. T data are limited in this region, but it is unlikely that halite would survive in M3/H3, only several meters from the Culebra, in regions of high T where Culebra flow rates are relatively high. High-T zones, therefore, are assumed to not occur in regions where halite is present in the M3/H3 interval.

TFIELD-3.5 Halite Bounding the Culebra

In regions where halite is present in the M2/H2 interval directly below the Culebra, no reliable quantitative estimates of Culebra T are available. Beauheim (1987) estimates T at P-18, the only tested well at which halite is present in the M2/H2 interval, to be less (probably much less) than 4×10^{-9} m^2/s ($\log_{10} = -8.4$). In much of the area where halite is present in the M2/H2 interval (including the P-18 location), halite is also present in the M3/H3 interval. Based upon geologic observations of halite-bound units elsewhere within the WIPP area, Holt (1997) suggests that porosity within the Culebra may contain abundant halite cements in these areas. Beauheim and Holt (1990) and Holt (1997) indicate that Culebra porosity shows increasing amounts of pore-filling cement east of the WIPP site. Consequently, Culebra T is assumed to be much lower in the region where halite occurs both above (M3/H3 interval) and below (M2/H2 interval) the Culebra. Much lower T is also assumed in the area northeast of the WIPP site where halite is present in the M2/H2 interval but absent in the M3/H3 interval (see Figure TFIELD-3).

TFIELD-3.6 High-T Zones

In addition to the high T that occurs everywhere dissolution of the upper Salado has occurred, high-T zones also occur in the Culebra in the region bounded by the limit of upper Salado dissolution to the west and by the margin of where halite is present in the M2/H2 and M3/H3 intervals to the east (see Figures TFIELD-2 and TFIELD-3). Fracture openness and interconnectivity in these high-T zones are controlled by a complicated history of fracturing with several episodes of cement precipitation and dissolution (Beauheim and Holt 1990; Holt 1997). No geologic metric has yet been defined that allows prediction of where fractures are filled or open, hence our knowledge of this indicator east of the Salado dissolution margin is limited to the test well locations shown in Figure TFIELD-6. Consequently, the spatial location of high-T zones between the Salado dissolution margin and the M2/H2 and M3/H3 margins is treated stochastically.

TFIELD-3.7 Linear Transmissivity Model

Using the hypothesized geologic controls on Culebra T, the following linear model for $Y(\mathbf{x}) = \log_{10} T(\mathbf{x})$ was constructed:

$$Y(\mathbf{x}) = \beta_1 + \beta_2\, d(\mathbf{x}) + \beta_3\, I_f(\mathbf{x}) + \beta_4\, I_D(\mathbf{x}) \qquad (2)$$

where β_i (i = 1, 2, 3, 4) are regression coefficients, $\mathbf{x}$ is a two-dimensional location vector consisting of UTM X and UTM Y coordinates, $d(\mathbf{x})$ is the overburden thickness, $I_f(\mathbf{x})$ is the fracture-interconnectivity indicator given in Equation (1) that assumes the value of 1 if fracturing and high T have been observed at point $\mathbf{x}$ and 0 otherwise, and $I_D(\mathbf{x})$ is a dissolution indicator function that assumes the value of 1 if Salado dissolution has occurred at point $\mathbf{x}$ and 0 otherwise. In this model, regression coefficient β_1 is the intercept value for the linear model. Coefficient β_2 is the slope of $Y(\mathbf{x})/d(\mathbf{x})$. Coefficients β_3 and β_4 represent adjustments to the intercept for the occurrence of interconnected fractures and Salado dissolution, respectively. Although other types of linear models could be developed, this model is consistent with the conceptual model relating T to geologic controls and can be tested using published WIPP geologic and T data. Note that the regression model does not explicitly contain terms relating Culebra T to zones where the Culebra is bounded by halite in both the M2/H2 and M3/H3 intervals because of lack of data from these areas. Therefore, it cannot be used to predict T east of the M2/H2 margin.

TFIELD-3.8 Linear-Regression Analysis

A linear-regression model was written using the Windows-based program Mathcad 7 Professional© specifically for this application. Although other variables are input, this model requires only $\log_{10}$ T data from tested wells, the depth of the Culebra at those wells, and an estimate of whether dissolution of the upper Salado has or has not occurred at each location. The fracture interconnectivity indicator is defined from the $\log_{10}$ T data, and a Salado dissolution indicator is defined using the Salado dissolution data. These data are then used in a standard linear regression algorithm to determine the regression coefficients for Equation (2).

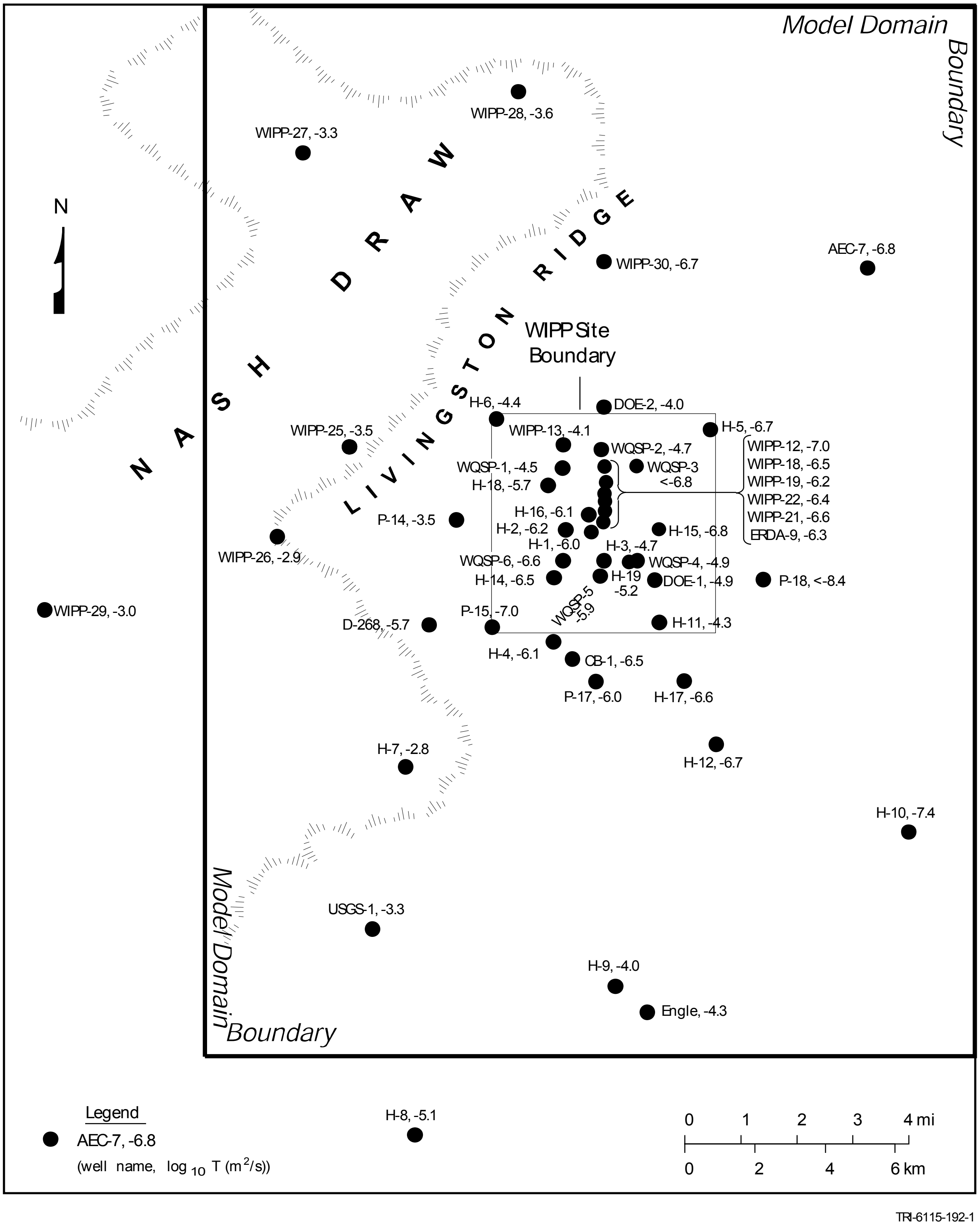

Figure TFIELD-6. Well Locations and Log_{10} Culebra Transmissivities

The regression coefficients for Equation (2) derived from this analysis are presented in Table TFIELD-1. The regression has a multiple correlation coefficient (R^2) of 0.941 and a Regression ANOVA F statistic of 222. The number of degrees of freedom about the regression (n) equals the number of observations (46) minus the number of parameters (4). The number of degrees of freedom due to the regression (m) equals the number of parameters (4) minus 1. With n = 42 and m = 3, the regression is significant above the 0.999 level. Residuals show no anomalous behavior. Accordingly, the regression model provides an accurate and reasonable description of the data. The fit of the regression to the $\log_{10}$ T data is shown in Figure TFIELD-7.

Table TFIELD-1. Regression Coefficients for Equations (2) and (3)

β_1	β_2	β_3	β_4
−5.441	-4.636×10^{-3}	1.926	0.678

The regression model does not predict T in the regions where the Culebra is underlain by halite in the M2/H2 interval because no quantitative data were available from these regions to be used in deriving the regression. In these regions, the following modified version of the regression model of Equation (2) is applied:

$$Y(\mathbf{x}) = \beta_1 + \beta_2\, d(\mathbf{x}) + \beta_3\, I_f(\mathbf{x}) + \beta_4\, I_D(\mathbf{x}) + \beta_5\, I_H(\mathbf{x}) \tag{3}$$

where $I_H(\mathbf{x})$ is a halite indicator function. This indicator is assigned a value of 1 in locations where halite occurs in the M2/H2 interval and 0 otherwise. The coefficient β_5 is set equal to −1 so that Equation (3) reduces the predicted T values by one order of magnitude where halite occurs in the M2/H2 interval, to accord qualitatively with the expected transmissivity reduction discussed in Section 3.5 of this attachment. With knowledge (or stochastic estimations) of the values of the geologic controls (e.g., Culebra depth, fracture-interconnectivity indicator, dissolution indicator, and halite indicator), Culebra T values can be predicted at unobserved locations in the WIPP Culebra model domain using Equation (3).

TFIELD-4.0 CALCULATION OF BASE T FIELDS

In this section, a method is developed for applying the linear regression model from Section 3.0 of this attachment to predict Culebra T across a model domain encompassing the WIPP area. Culebra overburden thickness, Salado dissolution, and the presence or absence of halite in units bounding the Culebra can be deterministically evaluated across the WIPP region using maps constructed from subsurface data (Section 2.0 of this attachment). The presence of open, interconnected fractures, however, cannot be deterministically assessed across the WIPP area using maps. A geostatistical approach, conditional indicator simulation, is used to generate 500 equiprobable realizations of zones with hydraulically significant fractures in the WIPP region. These simulations are parameterized using the frequency of occurrence of WIPP wells with hydraulically significant fractures and a fit to a variogram constructed using data from those same wells. The regression model is then applied to the entire WIPP area by:

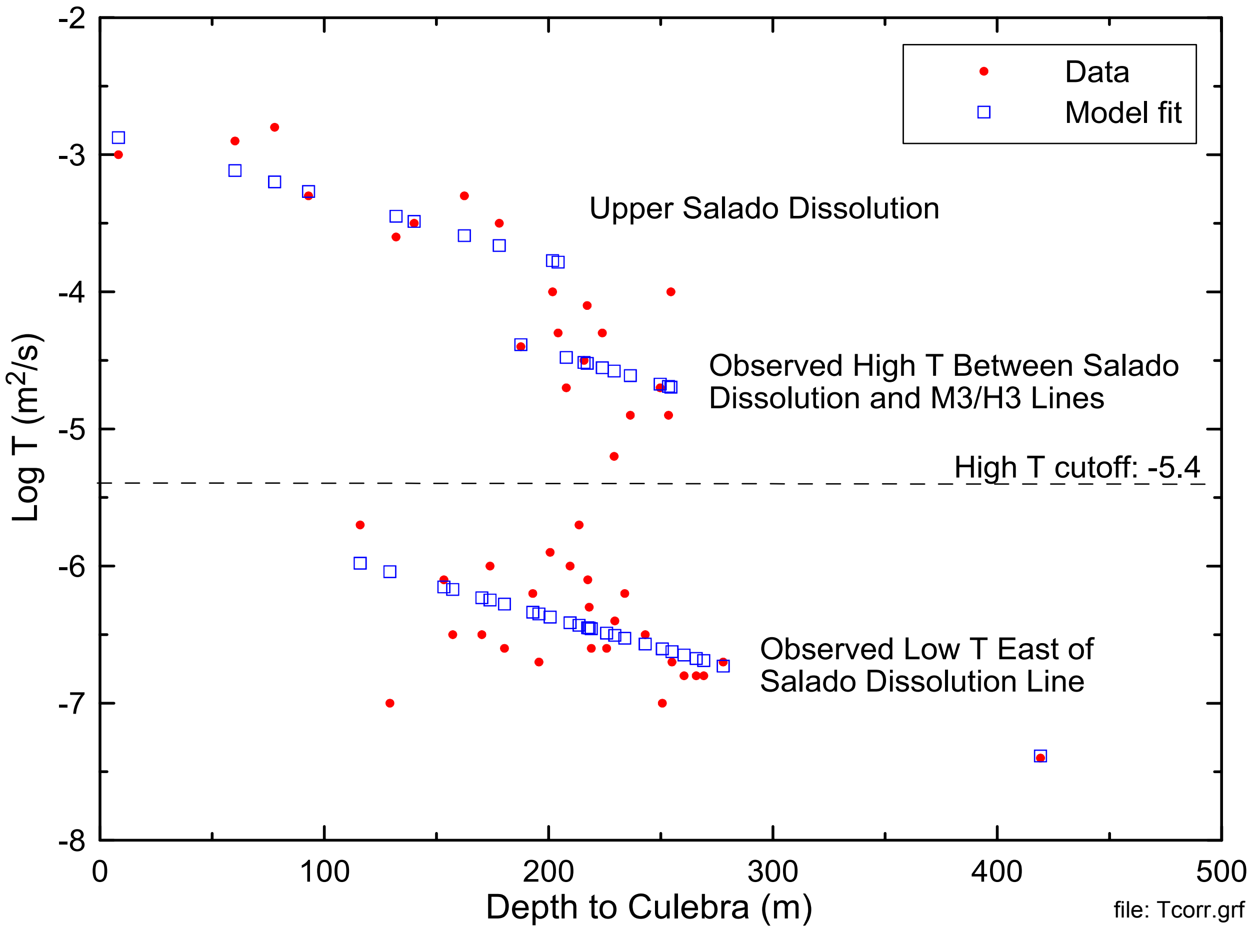

Figure TFIELD-7. Regression Fit to Observed Culebra Log_{10} T Data

1. Overlaying the geologic map data for Culebra overburden thickness, Salado dissolution, and the presence or absence of halite in units bounding the Culebra with each of the 500 equiprobable realizations of zones containing open, interconnected fractures.

2. Sampling each grid point within the model domain to determine the overburden thickness and the indicator values for Salado dissolution, overlying or underlying halite, and fracture interconnectivity.

3. Using the sampled data at each grid point with the regression model coefficients to estimate Culebra T.

When applied to the 500 equiprobable realizations of zones containing open, interconnected fractures, this procedure generates 500 stochastically varying Culebra base T fields. Details about the creation of the base T fields are given in Holt and Yarbrough (2002, 2003a, 2003b).

TFIELD-4.1 Definition of Model Domain

Two principal factors were considered in selecting the boundaries for the Culebra model domain. First, model boundaries should coincide with natural groundwater divides where feasible, or be far enough from the southern portion of the WIPP site, where transport will be modeled, to have minimal influence in that area. Second, the model domain should encompass known features with the potential to affect Culebra water levels at the WIPP site (e.g., potash tailings ponds). The modeling domain selected is 22.4 km (13.9 mi) east-west by 30.7 km (19.1 mi) north-south, aligned with the compass directions (Figure TFIELD-6). This is the same as the domain used by LaVenue et al. (1990) except that the current domain extends 1 km (0.62 mi) farther to the west than the 1990 domain. The modeling domain is discretized into 68,768 uniform 100-m (328-ft) by 100-m (328-ft) cells. The northern model boundary is slightly north of the northern end of Nash Draw, 12 km (7.5 mi) north of the northern WIPP site boundary and about 1 km (0.62 mi) north of Mississippi Potash Incorporated's east tailings pile. The eastern boundary lies in a low-T region that contributes little flow to the modeling domain. The southern boundary lies 12.2 km (7.6 mi) south of the southern WIPP site boundary, 1.7 km (1.5 mi) south of our southernmost well (H-9) and far enough from the WIPP site to have little effect on transport rates on the site. The western model boundary passes through the IMC tailings pond (Laguna Uno of Hunter [1985]) due west of the WIPP site in Nash Draw. Boundary conditions assigned for the model are discussed in Section 6.2 of this attachment. The coordinates of each corner of the domain are given in Table TFIELD-2*,* in NAD 27 UTM coordinates.

Table TFIELD-2. Coordinates of the Numerical Model Domain Corners

Domain Corner	UTM X Coordinate (m)	UTM Y Coordinate (m)
Northeast	624,050	3,597,150
Northwest	601,650	3,597,150
Southeast	624,050	3,566,450
Southwest	601,650	3,566,450

TFIELD-4.2 Reduction of Geologic Map Data

To create useable data sets for conditional simulation of high-T zones and prediction of Culebra T, the geological maps described above in Section 2.0 of this attachment were imported into a GIS environment and digitized. A uniform 100-m (328-ft) grid was then created over the Culebra model domain. Using the Culebra structure contour map data (Figure TFIELD-1) and surface elevation data obtained from the United States Geological Survey (USGS) National Elevation Dataset (NED) (http://edcnts12.cr.usgs.gov/ned), an isopach map of the Culebra overburden on the 100-m (328-ft) model grid was created.

Using maps showing occurrence of halite in the units above and below the Culebra and well locations, soft data files were created for conditional indicator simulations. T within 120 m (374 ft) of each well is assumed to be from the same population (e.g., high or low T reflecting open, interconnected fractures or filled (poorly interconnected) fractures, respectively), and regions where the Culebra is overlain by halite in M3/H3 or underlain by halite in M2/H2 are assumed to be low-T regions.

Using maps of Salado dissolution and the occurrence of halite in the units above and below the Culebra, 100-m (328-ft) indicator grids were created over the model domain. These indicator grids were created for regions affected by Salado dissolution, regions where the Culebra is underlain by halite in the M2/H2 interval, and a middle zone in which the Culebra is neither overlain nor underlain by halite where high-T zones occur stochastically (Figure TFIELD-8).

TFIELD-4.3 Indicator Variography

Excluding data where Salado dissolution occurs, Culebra T data are indicator transformed (1 for $\log_{10}$ T (m^2/s) > –5.4, 0 otherwise). A high-T indicator variogram is then constructed for the indicator data in the region not affected by Salado dissolution using the GSLIB program gamv (Deutsch and Journel 1998). The lag spacing for this variogram is selected to maximize variogram resolution. The resulting indicator variogram is then fit with an isotropic spherical variogram model:

$$\gamma(h) = \begin{cases} s[1.5(h/\lambda) - 0.5(h/\lambda)^3] & \text{if } h \leq \lambda \\ s & \text{if } h \geq \lambda \end{cases} \qquad (4)$$

where $\gamma(h)$ is the variogram as a function of lag spacing h, s is the sill value of the indicator variogram, and λ is the correlation length. This variogram model minimizes the mean squared error between the experimental and modeled variogram. The sill value was determined using:

$$s = P[\log_{10} T\,(\mathrm{m}^2/\mathrm{s}) > -5.4] - \{P[\log_{10} T\,(\mathrm{m}^2/\mathrm{s}) > -5.4]\}^2 \qquad (5)$$

For the Culebra data set, excluding wells where dissolution has occurred, $s = 0.201$. The correlation length λ was estimated to be 1,790 m (5,873 ft). No nugget effect was included in the variogram model (Figure TFIELD-9). Variogram model parameters were then used in conditional indicator simulations of Culebra high-T zones.

TFIELD-4.4 Conditional Indicator Simulation

"Soft" indicator data were created for the indicator simulations. To ensure that no high-T regions develop in areas where halite occurs in M2/H2 or M3/H3, soft data points, indicating low T, were placed on a 200-m (656-ft) grid east of the M2/H2 and M3/H3 salt margins. This 200-m (656-ft) grid used the original 100-m (328-ft) grid excluding every other node to assure the 200-m (656-ft) soft data grid spatially overlay the 100-m (328-ft) grid. Soft data were also specified for every 100-m (328-ft) node along the combined lines of the M2/H2 and M3/H3 salt margins.

Additional soft data were created near well locations establishing a 120-m (394-ft) buffer around each well (Figure TFIELD-10). All 100-m (328-ft) grid nodes lying within the 120-m (394-ft) buffer were selected and assigned the transmissivity attribute of the well. Because all the nodes within 120 m (394 ft) of the well and the node corresponding to the block containing the well were selected as soft data, there was duplication in the input files. Only one data point can occupy a 100-m (328-ft) grid space during a realization. Therefore, the node closest to the well was eliminated from the soft data file.

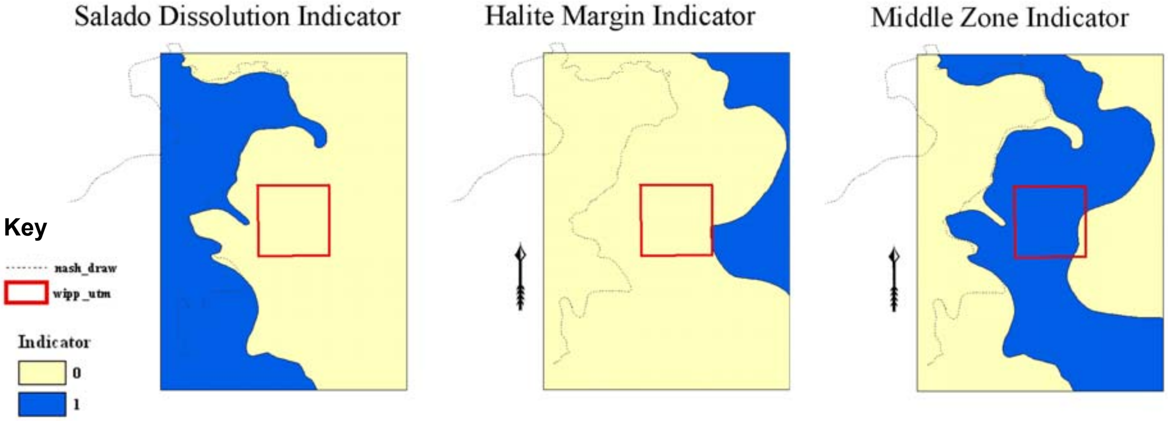

Figure TFIELD-8. Zones for Indicator Grids

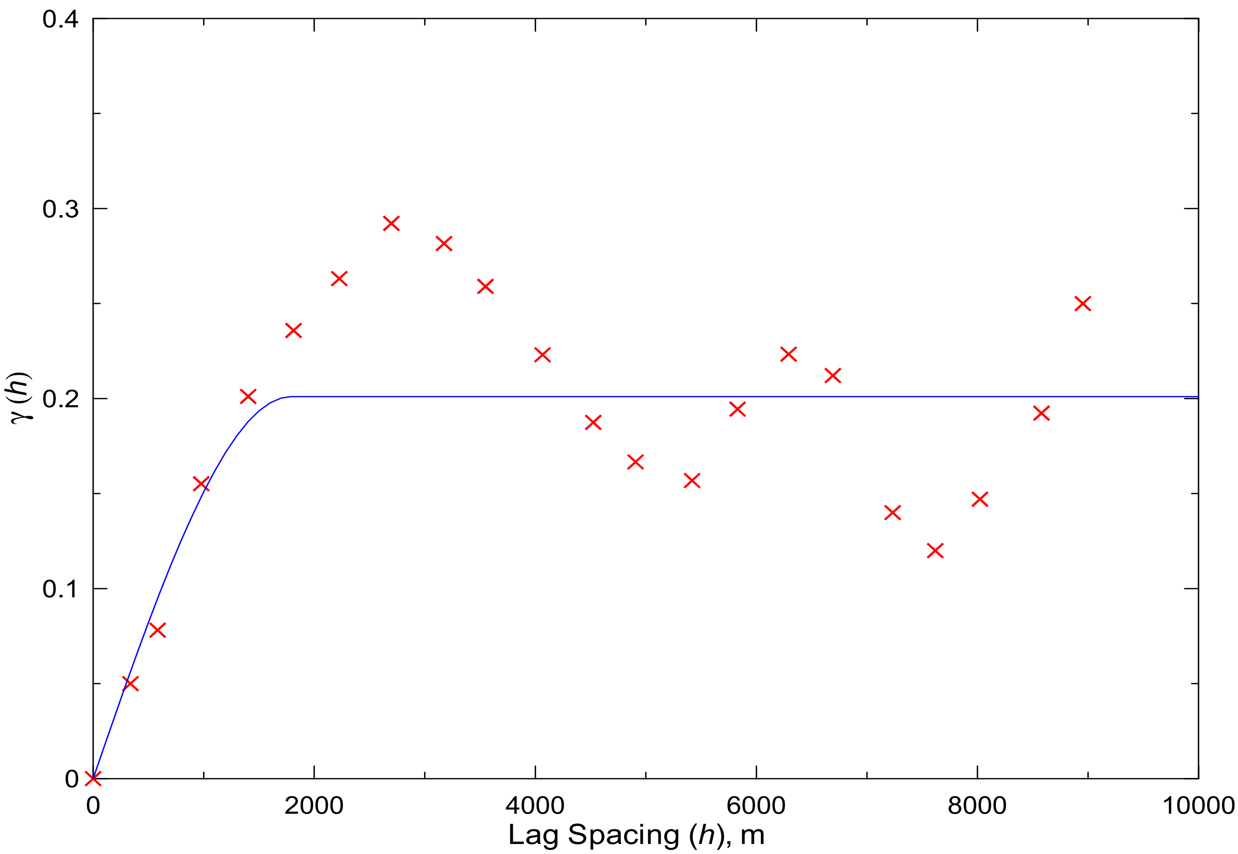

Figure TFIELD-9. High-T Indicator Model and Experimental Variograms

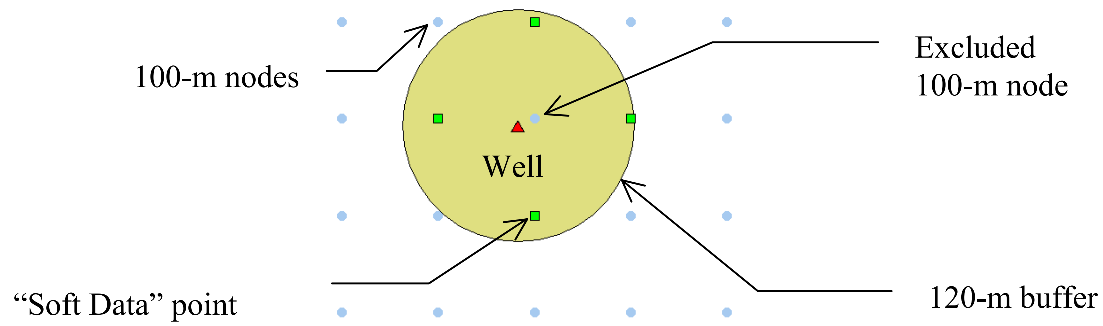

Figure TFIELD-10. Soft Data Around Wells

Five hundred conditional indicator simulations were generated on the 100-m (328-ft) model grid using the GSLIB program sisim (Deutsch and Journel 1998) with Culebra high-T indicator data, soft data for regions around wells and regions where halite underlies and overlies the Culebra, and the variogram parameters. The resulting indicator simulations were used in the construction of base T fields.

TFIELD-4.5 Construction of Base Transmissivity Fields

The linear predictor (Equation (3)) was used to generate 500 equally probable realizations of the T distribution in the Culebra model domain. This calculation required the regression coefficients discussed in Section 3.8 of this attachment, Culebra depth data (Section 3.9 of this attachment), a Salado dissolution indicator function, an indicator for where halite occurs in M2/H2, and the 500 realizations of high-T indicators discussed in Section 4.4 of this attachment.

The 500 base T fields were created in five sets. Each set consists of ten groups of ten realizations given d##r## designations. The "d" counter ranges from 01 to 50, while the "r" counter ranges from 01 to 10. An example base T field is shown in Figure TFIELD-11. Stochastically located patches of relatively high T (yellowish-green) can be clearly seen in the middle zone of the model domain. (Note: On black and white copy, these patches appear as the lightest shade of gray.)

TFIELD-5.0 CONSTRUCTION OF SEED REALIZATIONS

The base T fields described in Section 4.5 of this attachment rely on a regression model to estimate T at every location. By the nature of regression models, the estimated T values will not honor the measured T values at the measurement locations. Therefore, before using these base T fields in a flow model, they must be conditioned to the measured T values. This conditioning is performed with a Gaussian geostatistical simulation algorithm to generate a series of 500 spatially correlated residual fields where each field has a mean value of zero. These fields are conditional such that the residual value at each measurement location, when added to the value provided by the regression model (which is the same for all 500 fields), provides the known T value at that location. The result of adding the simulated residual field to the base T field is the "seed" realization.

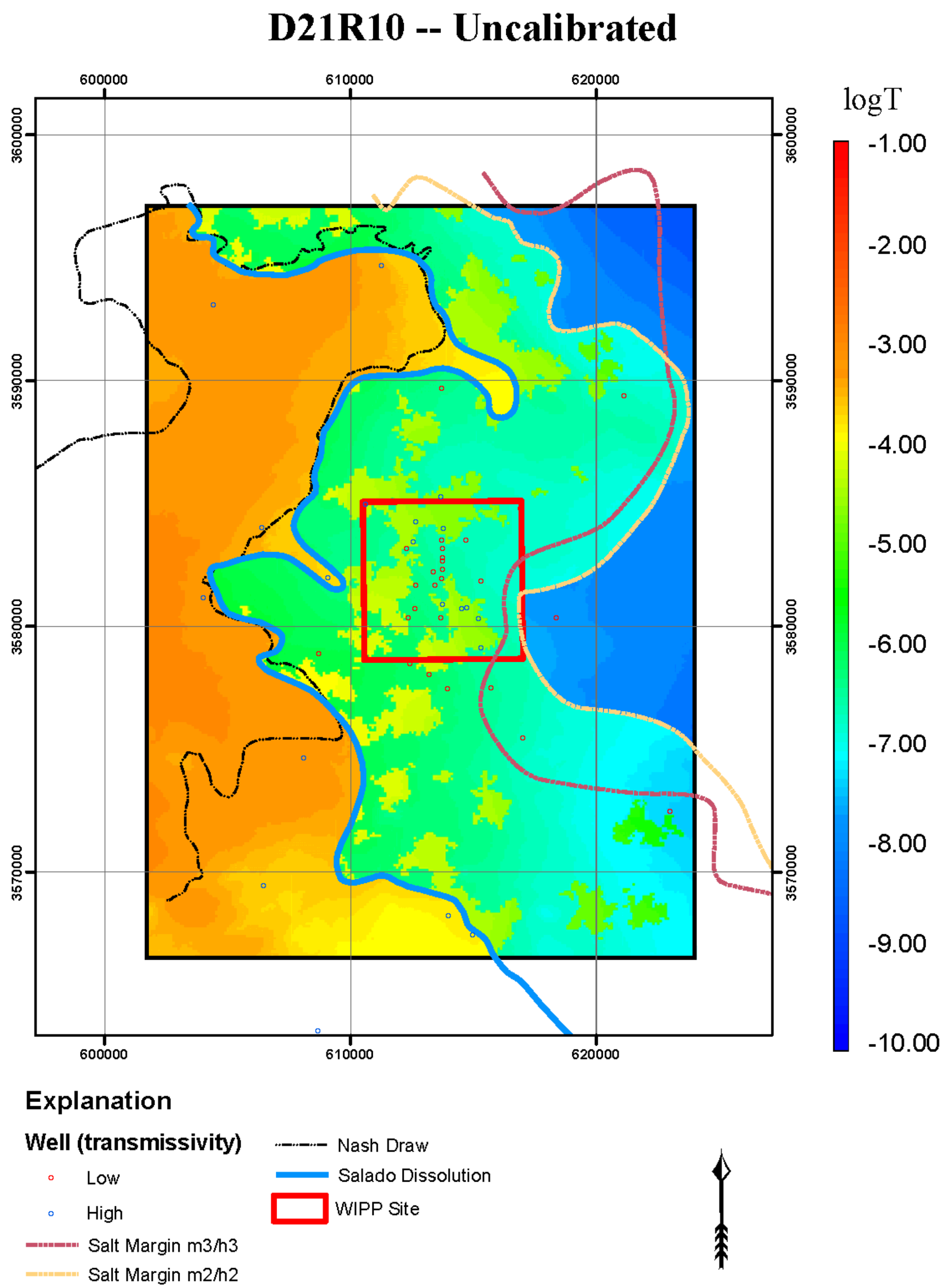

Figure TFIELD-11. Example Base T Field

This process is shown conceptually along a west-to-east cross section of the Culebra in Figure TFIELD-12. The upper image shows the value of the residuals at five T measurement locations across the cross section. These residuals are calculated as the observed (measured) T value minus the base field T value at the same locations. Positive residuals are where the measured T value is greater than that of the base T field. To create a T field from these residuals, there needs to be a way to tie the base field to the measured T values. This tie is accomplished by creating a spatial simulation of the residual values, a “residual field.” The middle image of Figure TFIELD-12 is an example residual field as a (red) dashed line along the cross section. This residual field is constructed through geostatistical simulation using a variogram model fit to the residual data. The residual field honors the measured residuals at their measurement locations and returns to a mean value of zero at distances far away from the measurement locations. Finally, this residual field is added to the base T field to create the seed T field. The base T field is represented by the solid (blue) line in the bottom image of Figure TFIELD-12 and the seed T field is shown by the dotted line. The seed T field corresponds to the base T field except at those locations where it must deviate to match the measured T data. The large discontinuity shown in the base T field at the bottom of Figure TFIELD-12 is due to the stochastic simulation of high-T zones within the Culebra.

A total of 46 measured T values and corresponding residual data, both in units of $\log_{10}$ (m^2/s), are available (Table TFIELD-3). For each pair of $\log_{10}$ T and residual data, the well name and the easting (X) and northing (Y) UTM coordinates are also given (for multiwell hydropads, a single well’s coordinates were used).

The process of creating the residual fields is to use the residual data to generate variograms in the VarioWin© software package and to then create conditional stochastic Gaussian geostatistical simulations of the residual field within the GSLIB program sgsim (Deutsch and Journel 1998).

To use the data in a Gaussian simulation algorithm, it is first necessary to transform the distribution of the raw residual data to a standard normal distribution. This is accomplished through a process called the “normal-score transform” where each transformed residual value is the “normal-score” of each original datum. The normal-score transform is a relatively simple two-step process. First the cumulative frequency of each original residual value, *cdf(i)*, is determined as:

$$cdf(i) = \frac{R(i) - 0.5}{N} \tag{6}$$

where *R(i)* is the rank (smallest to largest) of the i^{th} residual value and *N* is the total number of data (46 in this case). Then for each cumulative frequency value, the corresponding normal-score value is calculated from the inverse of the standard normal distribution. By definition, the standard normal distribution has a mean of 0.0 and a standard deviation of 1.0. Further details of the normal-score transform process can be found in Deutsch and Journel (1998).

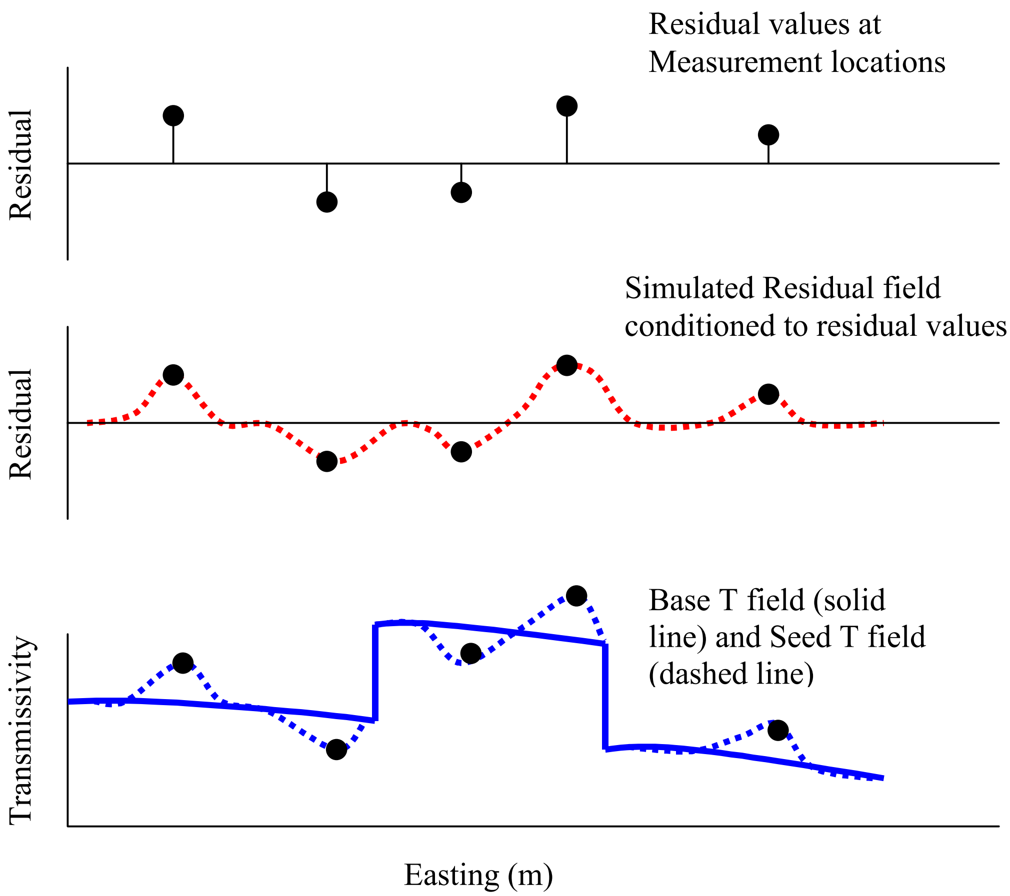

Figure TFIELD-12. Conceptual Cross Section Showing the Updating of the Residual Field and the Base T Field into the Seed T Field

Table TFIELD-3. Log_{10} Transmissivity Data Used in Inverse Calibrations

Well ID	Easting (UTM, m)	Northing (UTM, m)	$\log_{10}$ T (m^2/s)	$\log_{10}$ T residual (m^2/s)
AEC-7	621126	3589381	–6.8	–0.11078
CB-1	613191	3578049	–6.5	–0.32943
D-268	608702	3578877	–5.7	0.27914
DOE-1	615203	3580333	–4.9	–0.21004
DOE-2	613683	3585294	–4.0	0.69492
Engle	614953	3567454	–4.3	–0.51632
ERDA-9	613696	3581958	–6.3	0.15250
H-1	613423	3581684	–6.0	0.41295
H-2c	612666	3581668	–6.2	0.13594
H-3b1	613729	3580895	–4.7	–0.22131
H-4c	612406	3578499	–6.1	0.05221
H-5c	616903	3584802	–6.7	0.02946

Table TFIELD-3. Log_{10} Transmissivity Data Used in Inverse Calibrations — Continued

Well ID	Easting (UTM, m)	Northing (UTM, m)	log_{10} T (m^2/s)	log_{10} T residual (m^2/s)
H-6c	610610	3584983	–4.4	–0.01524
H-7c	608095	3574640	–2.8	0.39794
H-9c	613974	3568234	–4.0	–0.22763
H-10b	622975	3572473	–7.4	–0.01484
H-11b4	615301	3579131	–4.3	0.25314
H-12	617023	3575452	–6.7	–0.07647
H-14	612341	3580354	–6.5	–0.26934
H-15	615315	3581859	–6.8	–0.12631
H-16	613369	3582212	–6.1	0.34962
H-17	615718	3577513	–6.6	–0.14310
H-18	612264	3583166	–5.7	0.73159
H-19b0	614514	3580716	–5.2	–0.62242
P-14	609084	3581976	–3.5	0.16212
P-15	610624	3578747	–7.0	–0.95938
P-17	613926	3577466	–6.0	0.24762
USGS-1	606462	3569459	–3.3	0.28998
WIPP-12	613710	3583524	–7.0	–0.39627
WIPP-13	612644	3584247	–4.1	0.42180
WIPP-18	613735	3583179	–6.5	0.06840
WIPP-19	613739	3582782	–6.2	0.32598
WIPP-21	613743	3582319	–6.6	–0.11148
WIPP-22	613739	3582653	–6.4	0.10549
WIPP-25	606385	3584028	–3.5	–0.01378
WIPP-26	604014	3581162	–2.9	0.21598
WIPP-27	604426	3593079	–3.3	–0.03209
WIPP-28	611266	3594680	–3.6	–0.15124
WIPP-29	596981	3578694	–3.0	–0.12497
WIPP-30	613721	3589701	–6.7	–0.35131
WQSP-1	612561	3583427	–4.5	0.01540
WQSP-2	613776	3583973	–4.7	–0.02729
WQSP-3	614686	3583518	–6.8	–0.15139
WQSP-4	614728	3580766	–4.9	–0.28895
WQSP-5	613668	3580353	–5.9	0.47178
WQSP-6	612605	3580736	–6.6	–0.32261

The two-step normal-score transformation process is conducted in Microsoft Excel© (see details in McKenna and Hart 2003b). The resulting normal-score values are the distance from the mean as measured in standard deviations. The parameters describing the residual and normal-score transformed distributions are presented in Table TFIELD-4.

Table TFIELD-4. Statistical Parameters Describing the Distributions of the Raw and Normal-score Transformed Residual Data

Parameter	Raw Residual	Normal-Score Transformed Residual Data
Mean	0.000	0.000
Median	–0.015	0.000
Standard Deviation	0.330	0.997
Minimum	–0.959	–2.295
Maximum	0.732	2.295

The omnidirectional variogram is calculated with a 250-m (820-ft) lag spacing. The experimental variogram is shown in Figure TFIELD-13. The model fit to this experimental variogram is Gaussian with a nugget of 0.2, a sill of 0.8, and a range of 1,050 m (3,445 ft). The sum of the nugget and sill values is constrained to equal the theoretical variance of 1.0 by the sgsim software that is used to create the spatially correlated residual fields.

The variogram parameters for the normal-score transformed residuals are used directly in the sgsim program to create 500 conditional realizations of the residual field. Each of these 500 residual fields is used as an initial residual field and each one is assigned to an individual base T field. An example of a realization of the residual field and its combination with a base T field is shown in Figure TFIELD-14. From Figure TFIELD-14, the effect of the residual field on the base T field can be seen. The residual field perturbs the Ts to match the measured Ts at the well locations. The discrete features that are part of the original base T field (e.g., high-T zones in the middle of the domain) are retained when the residual field is added to the base field, although T values within those features may be altered to a degree.

A number of distributed locations within the modeling domain are selected and designated as "pilot points." PEST adjusts the T value at each of these pilot points to achieve a better match between the groundwater flow model results and the observed steady-state and transient head data. The adjustments in T at each pilot point cannot be made independently of surrounding T values and, therefore, these surrounding T values must be updated in a manner consistent with the change made at the pilot point. This updating is done by applying a change at each of the surrounding points that is a weighted fraction of the change made at the pilot point. The weights are calculated from the residual variogram.

These updates are necessary to create a final T field that honors all observed T measurements and matches the observed heads when used as input to a groundwater flow model. Therefore, it is also necessary to calculate and model a variogram on the raw, not normal-score transformed,

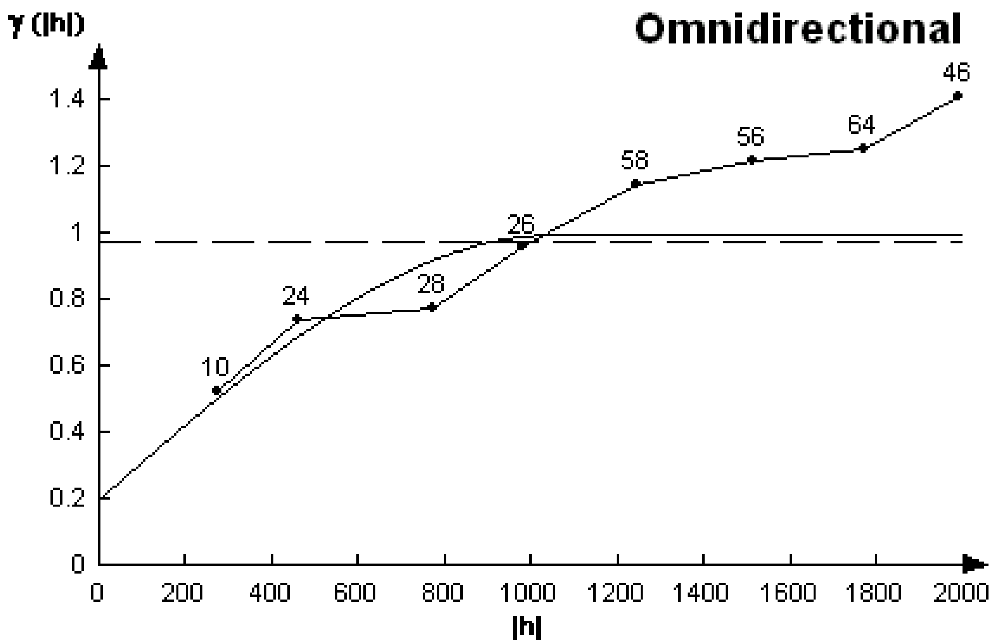

Figure TFIELD-13. Omnidirectional Variogram Model Fit to the Experimental Variogram of the Transmissivity Residuals

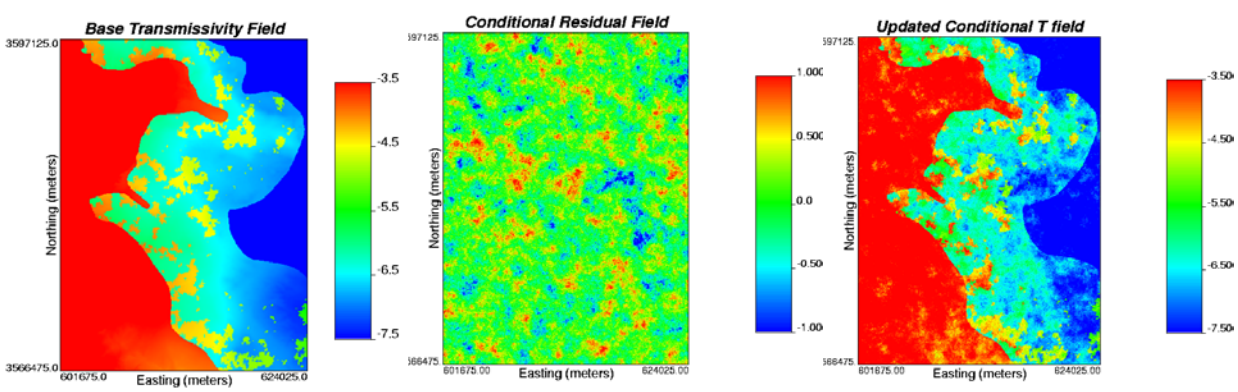

Figure TFIELD-14. An Example of the Creation of a Seed T Field. The base T field (left image) is combined with the initial residual field created through geostatistical simulation (center image) to produce the seed T field (right image). That field is then used as the initial field for the first iteration of the inverse calibration procedure. All three color scales denote the $\log_{10}$ T (m^2/s) value.

residuals for use in this kriging process. This variogram was also calculated with a 250-m (820-ft) lag and is omnidirectional. A doubly nested spherical variogram model was fit to the experimental variogram. The variogram parameters are a nugget of 0.008, a first sill and range of 0.033 and 500 m (1,640 ft), respectively, and a second sill and range of 0.067 and 1,500 m (4,921 ft), respectively (Figure TFIELD-15).

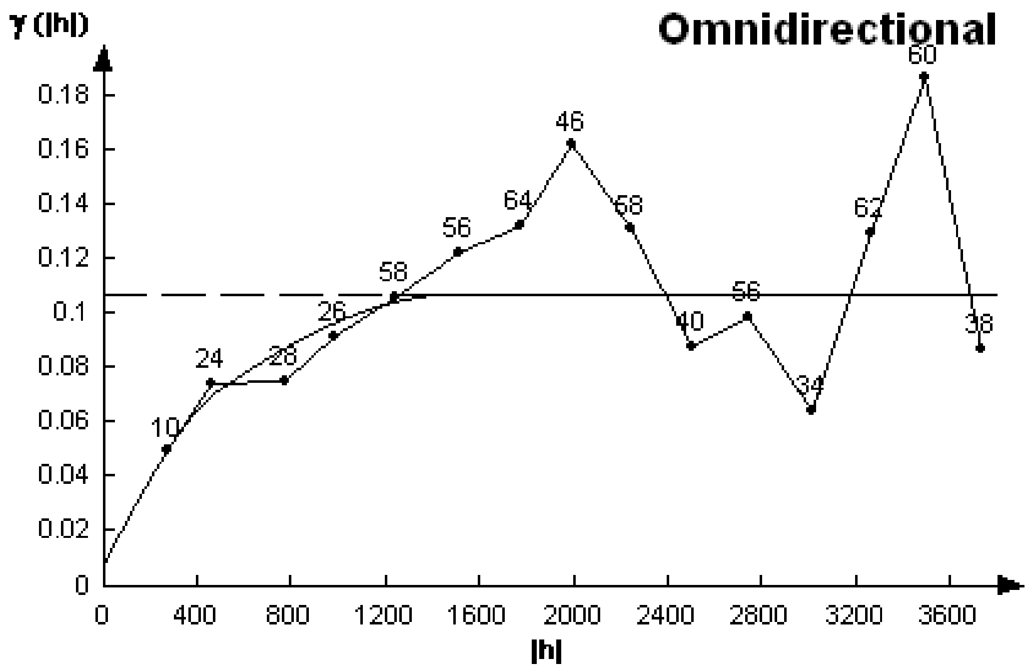

Figure TFIELD-15. Experimental and Model Variograms for the Raw-Space (Not Normal-Score Transformed) Transmissivity Residual Data

TFIELD-6.0 T-FIELD CALIBRATION TO STEADY-STATE AND TRANSIENT HEADS

This section presents details on the modeling approach used to calibrate the T fields to both the 2000 steady-state heads and 1,332 transient drawdown measurements. This section is divided into the following subsections:

1. Assumptions made in the modeling and the implications of these assumptions are provided.
2. The initial heads used for each calibration are estimated at each location in the domain using the heads measured in 2000 using kriging and accounting for the regional trend in the head values.
3. The initial heads are used to assign fixed-head boundaries to three sides of the model. The fourth side, the western edge, is set as a no-flow boundary for the model.
4. The transient head observations for each hydraulic test and each observation well are selected from the database. These heads are shown as a function of time for each hydraulic test.
5. The spatial and temporal discretization of the model domain are presented.

6. The transient head observations are given relative weights based on the inverse of the maximum observed drawdown in each hydraulic test. The relative weights assigned to the steady-state observations are also discussed.

7. The locations of the adjustable pilot points are determined using a combination of approaches.

All of these steps can be considered as preprocessing aspects of the stochastic inverse calibration procedure. The actual calibrations are done using an iterative coupling of the MODFLOW-2000 and PEST codes. The details of this process are covered in McKenna and Hart (2003a, 2003b), and are briefly summarized in this section.

TFIELD-6.1 Modeling Assumptions

The major assumptions that apply to this set of model calculations are:

1. The boundary conditions along the model domain boundary are known and do not change over the time frame of the model. This assumption applies to both the no-flow boundary along the western edge of the domain as well as to the fixed-head boundaries that were created to be consistent with the 2000 head measurements in the model domain. Implicit in this assumption is that the fixed-head boundary conditions do not have a significant impact on the transient tests that were simulated in the interior of the model at times other than the 2000 period.

2. The fracture permeability of the Culebra can be adequately modeled as a continuum at the 100-m (328-ft) × 100-m (328-ft) grid block scale and the measured T values used to condition the model are representative of the T in the 100-m (328-ft) × 100-m (328-ft) grid block in which the well test was performed. Implicit in this assumption is the prior assumption that the hydraulic test interpretations were done correctly and used the correct conceptual model.

3. Variable fluid densities in the Culebra can be adequately represented by casting the numerical solution in terms of freshwater head. Davies (1989) investigated the effects of variable fluid density on the directions of flow calculated in the Culebra using a freshwater-head approach. As the Culebra flow system was conceptualized and modeled by Davies, most of the water flowing in the Culebra in the vicinity of the WIPP site ultimately discharged to the Pecos River southwest of WIPP. When variable fluid density was taken into account, the only locations within the model domain where the flow direction changed by more than 10 degrees were regions 1.1 to 14.3 km (0.7 to 8.9 mi) south of the WIPP site, where the flow direction shifted as much as 70 degrees to the east toward a more downdip direction (but still primarily to the south) (Davies, 1989, Figures 35 and 36). As currently conceptualized, flow in the Culebra in the vicinity of WIPP does not discharge to the Pecos to the southwest, but instead goes to the southsoutheast toward the Paduca oilfield where extensive dissolution of the Salado and collapse of the Culebra has occurred (see Figure TFIELD-1). Hence, taking variable fluid density into account would have little effect on the flow direction.